

Contents lists available at ScienceDirect

Fuel

journal homepage: www.elsevier.com/locate/fuel



Full length article

Methyl methacrylate thermal decomposition: Modeling and laser spectroscopy of species time-histories behind reflected shock waves

Isabelle C. Sanders ^{a,*}, Nicholas M. Kuenning ^a, Nicolas Q. Minesi ^a, Daniel I. Pineda ^b, R. Mitchell Spearrin ^a

- ^a Department of Mechanical and Aerospace Engineering, University of California, Los Angeles (UCLA), Los Angeles, CA 90095, USA
- b Department of Mechanical Engineering, The University of Texas at San Antonio (UTSA), San Antonio, TX, 78249, USA

ARTICLE INFO

Keywords: Methyl methacrylate Methyl ester Pyrolysis Decomposition kinetics Absorption spectroscopy Time-history High temperature

ABSTRACT

The thermal decomposition of methyl methacrylate (MMA) was studied through species time-history measurements of formaldehyde (CH₂O), carbon monoxide (CO), and carbon dioxide (CO₂) behind reflected shock waves over a temperature range of 1200–1600 K near 1 atm. Tunable laser absorption spectroscopy was employed to spectrally and temporally-resolve a cluster of rovibrational lines in the Q-branches of the v_1 fundamental band and the v_2+v_4 combination band of CH₂O near 3.60 µm, three rovibrational transitions in the P-branch of the fundamental band of CO near 4.98 µm, and a transition in the R-branch of the $(01^00\rightarrow01^01)$ v_3 band of CO₂ near 4.19 µm. Spectral fitting procedures are subsequently used to infer CO, CO₂, and CH₂O mole fraction during the pyrolysis of shock-heated mixtures of MMA in argon. These data provided valuable experimental constraints on MMA pyrolysis chemical kinetic models. Sensitivity analysis of a detailed chemical model for MMA decomposition identified specific reactions likely to account for differences observed between the species measurements and simulations of the test conditions. Modified reaction rate parameters for select MMA decomposition reactions are proposed, determined via a genetic algorithm optimization procedure anchored to the speciation data.

1. Introduction

Poly methyl methacrylate (PMMA, also commonly referred to as acrylic glass) is a synthetic solid fuel of keen interest to both the fire science and propulsion communities [1-9]. In fire science, PMMA has recently been used as a baseline solid fuel to study flame spread in both normal [10] and reduced [11] gravity, with applications to material flammability for in-space missions. In propulsion, the stability of PMMA in long-term storage has motivated its investigation as both a hybrid rocket propellant [7,12] and for solid-fuel scramjet applications [13]. In both applications, knowledge of PMMA's regression rate - which is influenced heavily by local radiant heat flux and flow conditions - is critical to device safety, performance, and mission lifetime. Unlike many polymers, the pyrolysis kinetics of PMMA are not complicated by charring or cross-linking behavior and it involves relatively simple depolymerization behavior; its constituent monomer - methyl methacrylate (MMA, C₅H₈O₂) - accounts for over 90% of its pyrolysis products [3], providing a relatively tractable model for solid fuel combustion. However, the detailed reaction chemistry of the MMA monomer itself is not well-characterized, hindering the design and

modeling of next-generation hybrid combustion devices and advanced fire science experiments.

Existing models describing MMA reaction chemistry have been primarily developed during broader investigations of oxygenated hydrocarbon reaction kinetics. MMA belongs to a class of oxygenated compounds known as esters, specific types of which have received increasing attention in recent years owing to their potential to augment or replace conventional fossil-derived hydrocarbon fuels [14]. However, the pyrolysis and oxidation kinetics of many such esters are difficult to characterize in the laboratory owing to their high molecular weights and low vapor pressures [15-17]. For this reason, relevant experimental and computational research efforts have focused on smaller molecules with similar or analogous functional groups - including short-chain akyl esters like MMA - with the aim of providing kinetic insights on their long-chain counterparts. Examined esters which share reaction chemistry with MMA include acetates and formates [18,19], butanoates and propanoates [16,20], as well as crotonates, propenoates, and acrylates [15,17], among others.

However, previous chemical kinetic studies specifically involving MMA – which can provide modeling constraints specific to its molecular

E-mail address: isabellesanders@ucla.edu (I.C. Sanders).

^{*} Corresponding author.

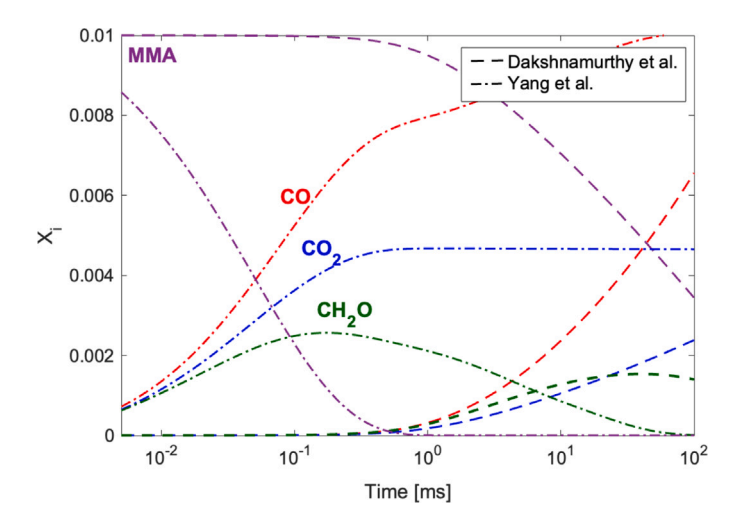


Fig. 1. Predicted combustion species evolutions at 1350 K from a 1% initial concentration of MMA diluted in argon at 1 atm using the chemical models published by Yang et al. (dot-dashed line) and Dakshnamurthy et al. (dashed).

structure – have been limited to laminar flame investigations [1,15,21–25]. Laminar flames provide useful validation benchmarks, but the convolution of transport mechanisms with pyrolysis and oxidation chemistry complicate the interrogation of specific reaction pathways, specifically the incipient fuel decomposition chemistry. Moreover, the kinetics of fuel pyrolysis and ignition are radically distinct from those of flames [26], wherein the destruction of the fuel molecules is achieved mainly through a convolution of thermal diffusion and H-abstraction reactions readily enabled by an abundance of radicals provided by the flame zone. To illustrate the shortcomings of reaction model optimization on the basis of laminar flames alone, time-resolved well-mixed constant pressure reactor simulations of MMA decomposition at 1350 K and 1 atm using two different chemical kinetic models are shown in Fig. 1.

The first chemical model shown, by Dakshnamurthy et al. [23], has been reduced from the second model shown by Yang et al. [15] and optimized for multidimensional reacting flow simulations of MMA combustion. In these chemical models, many Arrhenius reaction rate parameters relevant to MMA decomposition and oxidation have been estimated [20] or based on those of similar reactions of other molecules [23]. Notably, the two models disagree in their time-resolved species predictions by multiple orders of magnitude, despite both reasonably reproducing species profiles and flame speeds of laminar flames fueled by MMA [15,23].

To address these discrepancies, the predictive capability of fuel decomposition models can be evaluated in the laboratory through comparison with time-resolved species measurements behind reflected shock waves using optically-based measurement methods such as laser absorption spectroscopy (LAS) [27]. Notably, shock tube experiments can provide near homogeneous, isothermal conditions absent of transport phenomena, and may be used to study high-temperature chemical kinetics without oxidation chemistry. As such, shock tubes provide an ideal reactor for studies of thermal pyrolysis. When coupled with automated reaction model optimization [28–30], multiple Arrhenius rate parameters can be optimized simultaneously across multiple experiments performed at different temperatures, reducing the uncertainties in parameters that were hitherto estimated by functional group analogy or through ab-initio computational chemistry.

In this study, we investigate the reaction kinetics of methyl methacrylate decomposition at elevated temperatures (1200–1600 K) and near-atmospheric pressures behind reflected shock waves via time-resolved laser absorption measurements of $\rm CO$, $\rm CO_2$, and $\rm CH_2O$ mole fraction. We first present our experimental methodology, including

experimental shock tube apparatus, optical setup, and laser absorption spectroscopy, with specific attention to wavelength selection and data interpretation. We follow this with a presentation of our novel dataset capturing CO, CO2, and CH2O evolution alongside predictions of kinetic models targeting MMA reaction chemistry. A detailed analysis is performed examining the causes of disagreement between model predictions and experimental observations, identifying some key uncertain reactions in the models by performing sensitivity analyses of reactions with respect to predicted mole fractions of CO, CO2, and CH₂O. We modify multiple rate parameters of these identified reactions using an automated optimization procedure which seeks to minimize the discrepancies between the model predictions and experimental observations across all of the temperatures achieved in the experiments. The modified rate parameters are shown to yield significant improvement in predictive capability for time-resolved CO, CO2, and CH2O evolution during MMA decomposition. It is envisioned that the adjusted rate parameters will provide more accurate predictions in applications involving MMA for which chemical timescales are particularly relevant, such as in turbulent [31] and extinction [32] combustion regimes, which pervade propulsion and fire environments, respectively.

2. Experimental methods

2.1. Experimental setup

High-temperature chemical kinetics experiments in this study were performed in the High Enthalpy Shock Tube facility (HEST) at UCLA, described in previous work [33,34] and depicted in Fig. 2. The stainless steel shock tube comprises a 1.5-m high-pressure driver section and a 4.9-m low-pressure driven (test gas) section, separated by a polycarbonate diaphragm. The test section of the shock tube has a transverse optical pathlength of L = 10.32 cm and is circumscribed by interchangeable ports holding either sensors or optical windows, positioned axially 2 cm from the end wall. For all experiments, reflected shock pressure in the shock tube test section is measured directly with a dynamic pressure transducer (Kistler 601B1) via a charge amplifier (Kistler 5018 A) and post-shock temperature is inferred from the shock wave speed determined via time of arrival sensors (Dynasen, Inc.) along the shock tube. Uncertainty in reflected shock test conditions are typically about 1% when properly accounting for vibrational relaxation of all components of the test gas [35].

The shock tube is connected to vacuum pumps, an agitated mixing tank, and a gas delivery manifold used to barometrically prepare gas mixtures for all experiments using dual-capacitance heated manometers (MKS Baratron 627B). Notably, the gas delivery manifold is also connected to an interchangeable glass flask containing either solid or liquid chemicals from which gaseous vapors are evaporated and mixed with inert gases during preparation of the test gas mixtures. For studying the decomposition of MMA, mixtures of MMA in argon (Ar) were prepared by evaporating liquid MMA from the interchangeable glass flask into the agitated mixing tank to a desired partial pressure (below MMA's vapor pressure of ~29 Torr) and subsequently filling the tank with Ar. Prior to the preparation of each mixture and before each shock test, the inner surfaces of the mixing tank and shock tube driven section are passivated with MMA and the prepared MMA/Ar mixture, respectively, after which the mixing tank and shock tube test section are vacuumed and filled to the desired fill pressure. The procedure specifics were developed such to mitigate adsorption of MMA from the test gas mixture into the walls.

2.2. Laser absorption spectroscopy

Laser absorption spectroscopy (LAS) is a well-established optical diagnostic technique for shock tube kinetics studies, owing to its high time-resolution, species specificity, and quantitative capability in the measurement of species and temperature [27]. Spectral absorbance

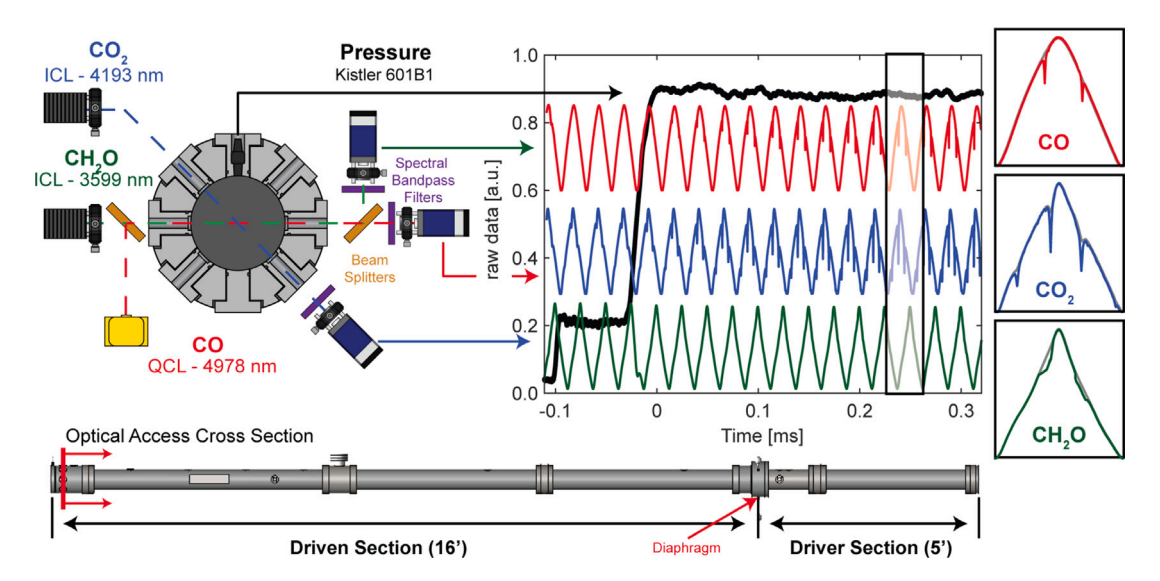


Fig. 2. (Top left) Cross sectional view of HEST facility showing optical access and laser/detector setup. (bottom) Side view of HEST facility marking location of cross section at the end of the driven section on the left. (Top right) Representative time histories of pressure (black), formaldehyde (green), CO (red), and CO₂ (blue) from shock heated mixture of MMA. (For interpretation of the references to color in this figure legend, the reader is referred to the web version of this article.)

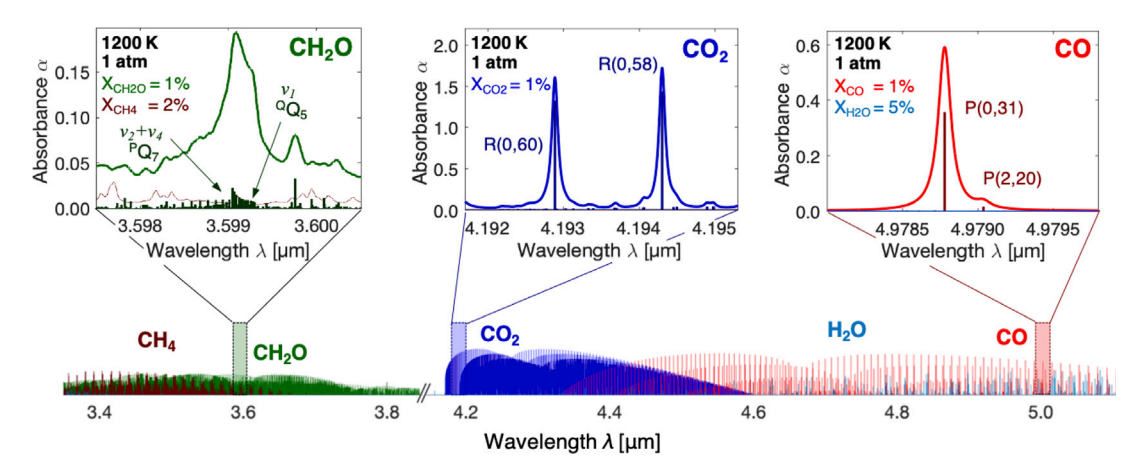


Fig. 3. Bottom: Absorption linestrengths for CH₄, CH₂O, CO₂, H₂O, and CO at 1200 K, simulated using the HITRAN [36] and HITEMP [37] databases. Top: Absorption simulations for CH₂O (left), CO₂ (middle), and CO (right), highlighting targeted wavelength regions and spectral features. CH₂O absorption simulated using the AYTY line list [38].

 $\alpha(\nu)$ of species measured in this work is calculated using the ratio of transmitted light (I_t) to incident light (I_0) at wavenumber ν [cm⁻¹] as defined by two different forms of the Beer–Lambert law:

$$\alpha(v) = -\ln\left(\frac{I_t}{I_0}\right)_v = PX_{abs}S_i(T)\varphi_i(v)L$$

$$= \sigma_{abs}(v, P, T)LN_{abs}$$
(1)

In the first form, P [atm] is the total pressure, $X_{\rm abs}$ is the absorbing species mole fraction, $S_i(T)$ [cm⁻²/atm] is the linestrength for rovibrational transition i at temperature T [K], and L [cm] is the absorption pathlength. In the second form, $\sigma_{\rm abs}(v,P,T)$ [cm²/molec.] is the absorbing species cross-section (dependent on v, P, and T), and $N_{\rm abs}$ [molec./cm³] is the absorbing species number density. The first form, used here to evaluate temperature and concentration of CO and CO₂, is typically employed when a comprehensive line-by-line spectral database of an absorbing species is confidently known and the spectral transitions i are easily separable in the absorbance measurement [8].

The second cross-section formulation of the Beer–Lambert law is appropriate for broadly-absorbing species for which the temperature-dependent line-by-line spectroscopy are less well-known and/or the absorbance spectra are convoluted enough to preclude identification of individual spectral transitions from the absorbance measurement.

In this study, we employ this second form of the Beer–Lambert law to quantitatively evaluate the temperature and concentration of formaldehyde, CH_2O , using a database of spectrally-resolved cross-sections $\sigma_{abs}(v,P,T)$ at multiple pressures and temperatures detailed in a separate work [39]. Spectroscopic measurements of CO and CO_2 are simultaneously performed with line-by-line interpretation.

An interband cascade laser (ICL, Nanoplus) with ${\sim}8.3$ mW of output power is used to target absorbance features of CH $_2$ O near 3.60 μm , while an ICL (Nanoplus) with ${\sim}6$ mW of output power targets CO $_2$ absorption features near 4.19 μm and a quantum cascade laser (QCL, ALPES Lasers) with ${\sim}50$ mW of output power targets CO absorbance features near 4.98 μm . Fig. 2 shows the optical setup in which the output light from each laser is pitched through the shock tube test section, spectral bandpass filters, irises, and focusing lenses onto photovoltaic (PV) detectors (VIGO Photonics).

The targeted spectral regions for each of the species measurements are shown in Fig. 3. The ICL used for CH₂O provides a scan depth of 1.03 cm⁻¹ at 40 kHz over a spectral range surrounding a collection of lines near 2778.5 cm⁻¹ comprising the $^{\rm Q}{\rm Q}_5$ branch of the v_1 symmetric C–H stretch band and the $^{\rm P}{\rm Q}_7$ branch of the v_2+v_4 combination band of CH₂O [40]. Likewise, the ICL targeting CO₂ provides a scan depth of 1.25 cm⁻¹ over the R(0,60) line of CO₂'s $(01^00 \rightarrow 01^01)$ v_3 fundamental band near 2385 cm⁻¹, while the QCL provides a scan depth

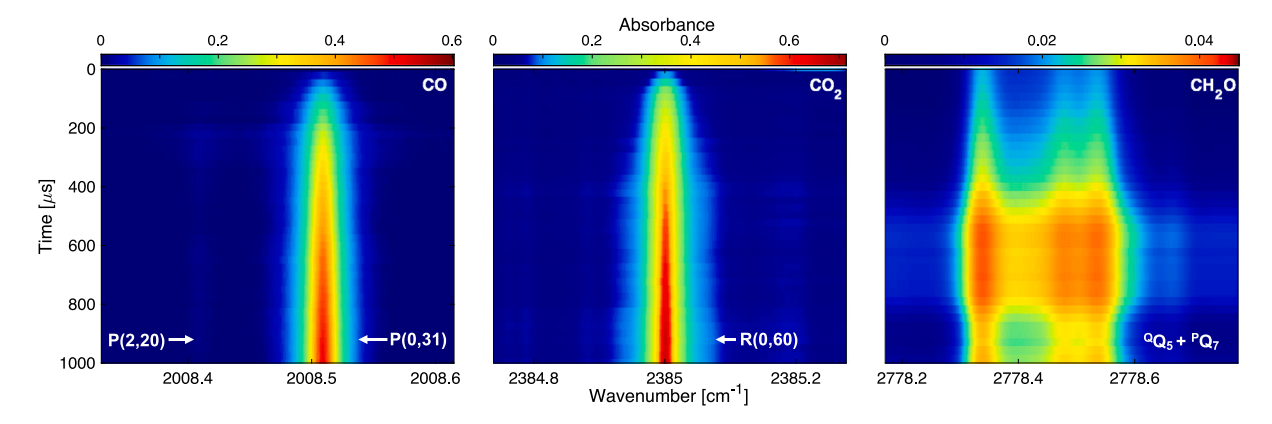


Fig. 4. Time evolution of absorbance of CO, CO₂, and CH₂O shown for a test at mid-range condition ($T_5 = 1390 \text{ K}, P_5 = 0.98 \text{ atm}$).

of 1.45 $\rm cm^{-1}$ over the P(0,31) and P(2,20) lines of CO's fundamental band near 2008.5 $\rm cm^{-1}.$

All lasers are scanned at 40 kHz using a triangle wave; representative scans for both the incident (I_0) and transmitted (I_t) intensity of each laser are shown in the right of Fig. 2 alongside a corresponding dynamic pressure measurement. The measured absorbance over 1 ms of post-shock test time is shown for each of CO, CO₂, and CH₂O in Fig. 4. The detection limits for tests over 1200 K to 1600 K for CO, CO₂, and CH₂O ranged from 5-10 ppm, 10-20 ppm, and 50-90 ppm, respectively. Following the procedure described in [8], the CO and CO2 spectra at each scan or time-step are fit assuming Voigt lineshape profiles [41] using spectral information from the HITEMP database with absorption areas, collisional widths, and linecenters as free parameters [37]. The measured CH₂O spectra are fit against the temperature-dependent cross-section database of Kuenning et al. by fixing temperature (via two-line thermometry of the CO and CO₂ spectra) and pressure (from pressure transducer) and with mole fraction as a free parameter [39].

3. Results

Shock tube experiments were conducted with 1% MMA near 1 atm (0.88 atm–1.10 atm) at initial post-shock temperatures in the range 1200–1600 K. Mole fraction time-histories for the three species measured in this work are shown in Fig. 5 for two representative experiments at different temperatures, along with corresponding predictions by the chemical models of Yang et al. [15] and Dakshnamurthy et al. [23]. Mole fraction time-history predictions are simulated by assuming the measured reflected shock temperature T_5 , pressure P_5 , and gas composition as the prescribed initial conditions in a constant pressure well-stirred reactor model. Representative error bars are

shown for uncertainty in measured species time histories and were calculated by propagating the uncertainty in measured temperature, reference-temperature transition linestrength (for CO and CO $_2$), absorption cross-section (for CH $_2$ O), and the reflected shock temperature and pressure, as in previous shock tube studies [33,34]. The average relative uncertainties in measured mole fractions of CO and CO $_2$ were 9% and 6%, respectively. For CH $_2$ O, the average relative uncertainty was ~25% due to uncertainty in the cross-sections used to calculate mole fraction and weak relative signals. For this reason we primarily employ the CO and CO $_2$ measurements to guide the rate parameter modification (discussed later) and use the CH $_2$ O data as a supplementary tool for validation.

The measurements deviate significantly from the predictions by both models with respect to CO and CO_2 mole fraction, with the detailed model by Yang et al. [15] over-predicting the production of CO and CO_2 , and the reduced model by Dakshnamurthy et al. [23] underpredicting the production of all measured species. Notably, measurements of $\mathrm{CH}_2\mathrm{O}$ show modest to good agreement with the magnitude of mole fraction predictions by the detailed model of Yang et al. However, the detailed model predicts rapid $\mathrm{CH}_2\mathrm{O}$ formation followed by slow depletion above $T_5 \approx 1230$ K, whereas this behavior is only observed experimentally at conditions above $T_5 \approx 1390$ K.

The observed temperature dependence of this species production and destruction is better predicted using a modified version of the reduced model presented here (described in Section 4), despite residual discrepancy in magnitudes at the highest temperatures. We provide detailed discussion on the methodology of the rate parameter adjustments in the development of our modified version of the chemical model in Section 4; however, we include the modified model predictions in this section for reader convenience and to avoid redundancy in figure content.

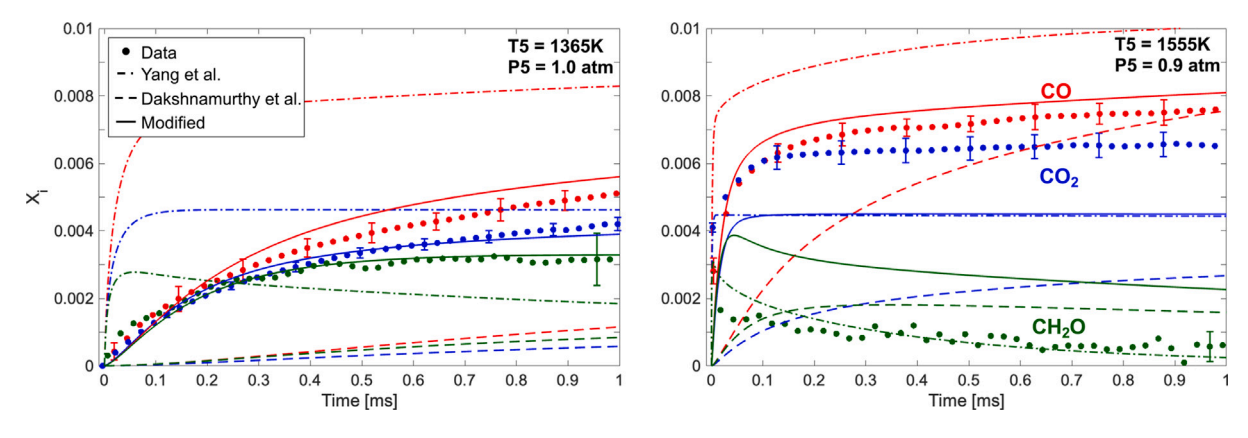


Fig. 5. Comparison of measured CO, CO₂, CH₂O mole fractions with simulations using the short MMA mechanism from Dakshnamurthy et al. (dashed line), the full mechanism from Yang et al. (dot-dashed line), and the modified mechanism from the current work (solid line).

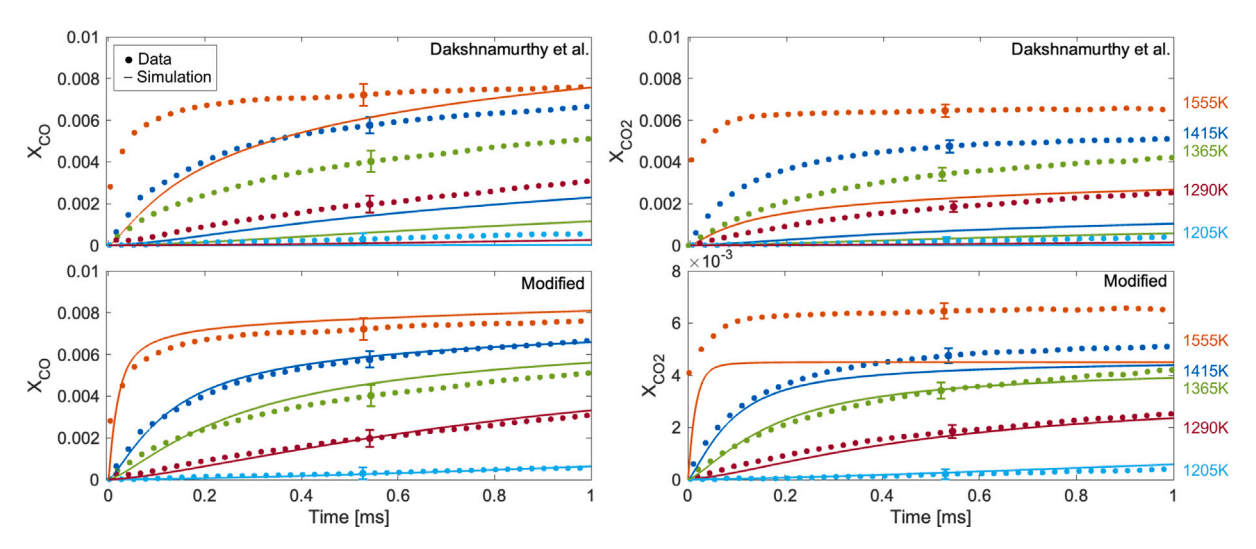


Fig. 6. Comparison of measured CO and CO₂ mole fractions with simulations (solid lines) using the short MMA mechanism from Dakshnamurthy et al. (top) and the modified mechanism from the current work (bottom).

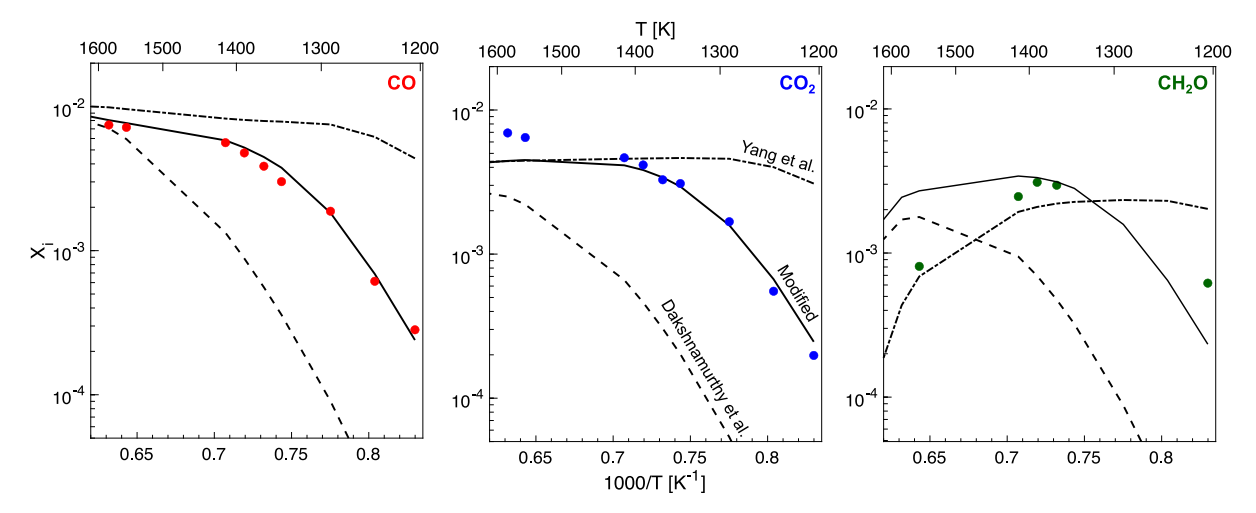


Fig. 7. Mole fraction yield for CO, CO₂, and CH₂O at 0.5 ms for 1% MMA/Ar pyrolysis. Markers represent measurements and lines represent the Yang et al. [15], Dakshnamurthy et al. [23], and final modified models.

Measured species time histories at multiple different initial temperatures are plotted in Fig. 6 for CO and CO2, alongside predictions using both the reduced model by Dakshnamurthy et al. [23] and our modified version of that model. As discussed in Section 4, we anchored the rate parameter optimization to the mole fractions time-histories of both CO and CO2 while the CH2O data, where available, served as a valuable additional benchmark for independent verification. Across all temperatures examined, CO and CO2 are produced in measurable quantities immediately post-shock at formation rates that increase with increased initial temperature T_5 . At low temperatures ($T_5 < 1400 \text{ K}$), CO and CO2 are observed to increase monotonically during the measured test time (~1 ms), while at higher temperatures, a plateau in yield is observed, wherein the mole fractions of CO and CO2 both increase rapidly, and subsequently increase more slowly for CO while nearly stagnating for CO2. The experimentally observed leveling off of CO2 supports the hypothesized reaction pathways of both the detailed and reduced models, which predict CO2 formation relatively early in MMA decomposition [15,23], despite its traditional role as a final product in combustion. Within the measurement test time, this transition point in kinetic behavior is predicted by the Dakshnamurthy et al. model to occur at higher temperatures than were observed experimentally, whereas the Yang et al. model predicts this trend transition at lower temperatures.

Fig. 7 shows the measured mole fraction of CO, CO2, and CH2O at 0.5 ms post-shock as a function of temperature compared to predictions from the three models considered in this work. Improved agreement is achieved across the measured temperature range for CO and CO₂ mole fractions with our modified model. Starting from 1200 K, CO and CO2 yields increase rapidly with temperature until a temperature threshold for trend transition is reached near 1400 K, above which the CO and CO2 yield increase more slowly. As temperatures approach the higher end of the measured range, the three models converge in prediction of CO and CO₂, highlighting the value of data at lower temperatures (T_5 < 1400 K) where model predictions more distinctly diverge. For $T_5 = 1500-1600$ K, both the Yang et al. and modified models predict a more dramatic plateau in CO2 mole fraction than is observed experimentally, while the Dakshnamurthy et al. model underpredicts the mole fraction most significantly. The measured CH₂O yield initially increases with temperature, peaks around $T_5 \approx 1390$ K, then decreases with further increasing temperature. The models all predict a similar trend, albeit with different temperature ranges governing this trend. The Yang et al. and Dakshnamurthy et al. models both predict a lower peak CH2O yield than observed, with the Yang et al. model suggesting peak yield at a lower temperature and the Dakshnamurthy et al. model predicting peak yield at a higher temperature than observed. The modified mechanism more closely matches the peak yield

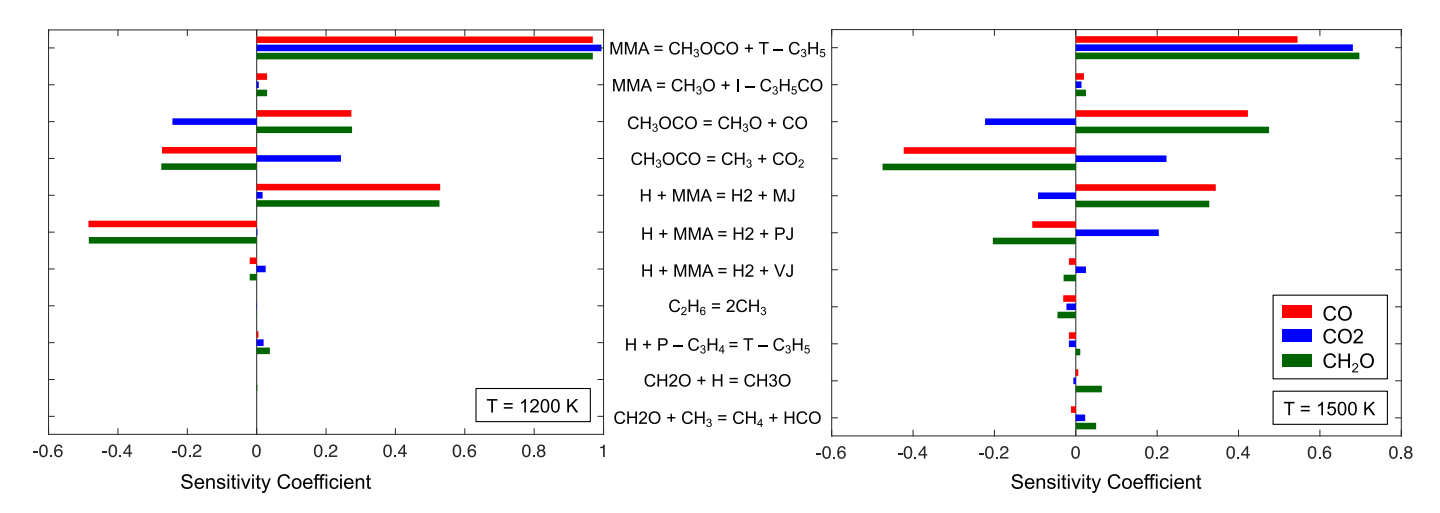


Fig. 8. Sensitivity coefficients for 1% MMA in argon at $P_5 = 1$ atm using the Dakshnamurthy et al. mechanism are shown at 0.1 ms for temperatures of 1200 K (left) and 1500 K (right). Reactions showing positive sensitivity factors increase species production.

magnitude and temperature. With the exception of the mole fraction yield recorded near $T_5=1550~\rm K$, the modified model most effectively reproduces the measured CH₂O yield, despite not being included as a speciation target in the mechanism optimization.

4. Kinetic modeling

In this section, we discuss the reaction kinetics of MMA decomposition and analyze chemical models for this kinetic behavior in context of the results presented in the previous section. We first briefly review existing kinetic models describing MMA reaction chemistry by Yang et al. [15] and Dakshnamurthy et al. [23]. We describe our methodology for using sensitivity analyses alongside descriptions of relevant initial MMA decomposition reactions and subsequent reaction pathways, from which a few key reactions were selected for adjustment. Modified rate parameters to these key reactions are proposed, via an optimization process anchored to time-resolved CO and ${\rm CO}_2$ speciation data

4.1. Decomposition pathway analysis

The detailed model by Yang et al. was developed during the study of three C5 unsaturated esters - including MMA - anchored to species mass spectrometry measurements in sub-atmosphere premixed flames [15,20]. This model includes 411 species and 2926 reactions. In general, the Yang et al. model shows accelerated species formation relative to experimental speciation trends, most notable at the lower end of the temperature range studied. This is clear in the 1365 K condition in Fig. 5. Such accelerated species formation at a given temperature suggests that the activation energies for reactions related to MMA decomposition may be underestimated in the detailed model. Such was the observation of Dakshnamurthy et al. in the development of their reduced model [23] optimized against laminar flame experiments; the activation energies for reactions related to MMA decomposition were increased and other reactions were adjusted as part of their model optimization based on recommendations from the literature. Several adjustments to rate parameters were based on those of similar reactions of methyl butanoate [42-45], methyl tiglate [46], methyl-2-methyl but-3-enoate [47], isobutene [48–50], 1-butene [51], methyl-2-butenoate [52], the isobutenyl radical [53], as well as propyne and allene [54]. The reduced model of Dakshnamurthy et al. also incorporated a base chemistry from Narayanaswamy et al. [55] to achieve accurate predictions for laminar burning velocities of not only MMA, but of smaller hydrocarbons as well. The mechanism, therein referred to as "short MMA mechanism", consists of 1084 reactions and 88 species. We focus here on optimizing the model against our time-resolved speciation measurements and proposing modified rate parameters for select reactions included in their short MMA mechanism.

We identify the reactions to which CO, $\rm CO_2$, and $\rm CH_2O$ concentrations are most sensitive using a time-resolved sensitivity analysis in an idealized reactor model in Cantera [56]. Although we use the Dakshnamurthy et al. mechanism as our base model for optimization, we also applied our sensitivity analysis to the detailed chemical model by Yang et al. [15], with all 411 species and 2926 reactions to ensure no crucial reactions were missed as many reaction pathways are often eliminated in a mechanism reduction. For completeness, we performed this analysis over the full range of post-shock initial temperatures in this study.

As a first step, a constant UV reactor model is used to screen for sensitive reactions in the existing models, initiated with the experimentally-determined reflected shock conditions T_5 and P_5 , as well as the molar composition X. We use the reactions and rates of the short MMA mechanism and rank the reactions by their sensitivity with respect to CO, CO2, and CH2O, and consider the top 50 in a subsequent sensitivity analysis utilizing the measured shock tube pressure and post-shock temperature in a split-timestep reactor model described in previous work [57], wherein non-reacting gas temperature changes caused by pressure rise or fall during the experiment are modeled via isentropic compression or expansion, respectively. The resulting sensitivity coefficients for reactions with high sensitivity for some or all of the three targeted species in the Dakshnamurthy et al. model are shown in Fig. 8. This analysis indicates that the targeted species sensitivity is heavily dominated by a small number of reactions. Notably, the H-abstraction reactions are more sensitive for CO and CH₂O at 1200 K, while more sensitive for CO₂ at 1500 K. We use these analyses to identify key reactions for rate parameter modification, informed by the LAS measurements. The first two reactions listed in Fig. 8 are the two unimolecular decomposition pathways of MMA:

$$MMA \iff iC_3H_5CO + CH_3O$$
 (R1)

$$MMA \iff tC_3H_5 + CH_3OCO$$
 (R2)

The reaction leading to CH_3OCO production (R2) is the most sensitive of all reactions included in the mechanism and significantly more sensitive for these species than (R1). The sensitivity coefficients are positive for CO, CO_2 , and CH_2O for both of these reactions indicating that rate increases will lead to increased production of all three molecules.

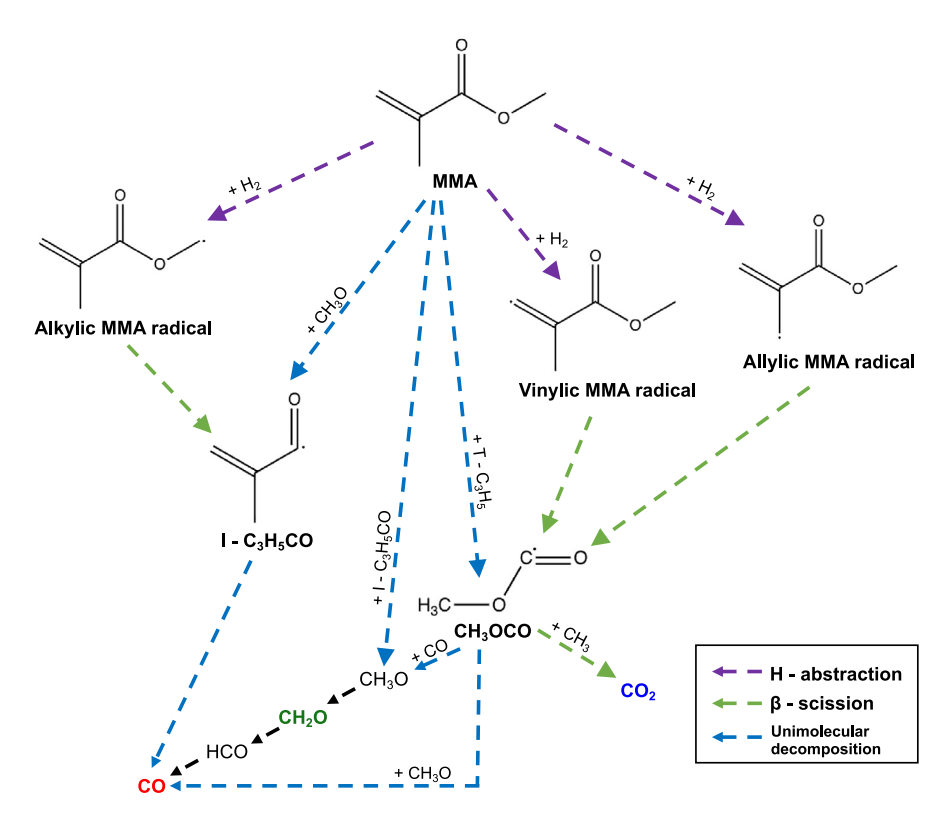


Fig. 9. MMA decomposition pathways considered in this work.

The next two reactions listed involve the decomposition of CH₃OCO:

$$CH_3OCO \longrightarrow CH_3O + CO$$

$$CH_3OCO \rightarrow CH_3 + CO_2$$

The sensitivity coefficients for these reactions notably indicate inverse relationship of species formation for CO and CH_2O versus CO_2 . The first reaction directly produces CO as well as CH_3O , which is a precursor to formation of CH_2O and CO; the second reaction produces CO_2 . Thus the relative rates between these two pathways will affect the ratio of CO (and CH_2O) to CO_2 formed. Despite the high sensitivity of these reactions, we omit them from our rate parameter modification, as these reactions have been studied more extensively in the literature [16,23].

The three reactions following ((R3) through (R5)) are the hydrogen abstraction reactions of MMA with atomic hydrogen, resulting in the respective allylic (PJ), alkylic (MJ), and vinylic (VJ) MMA radicals:

$$H + MMA \leftrightarrow H_2 + CH = C(CH_3) - C(=O) - O - CH_3 (PJ)$$
 (R3)

$$H + MMA \leftrightarrow H_2 + CH_2 = C(CH_3) - C(=O) - O - CH_2 (MJ)$$
 (R4)

$$H + MMA \leftrightarrow H_2 + CH_2 = C(CH_2) - C(=O) - O - CH_3 (VJ)$$
 (R5)

CO and $\mathrm{CH_2O}$ are also positively sensitive to the reactions (R3)–(R4). Note that abstractions by O and OH radicals, which are more relevant in oxidation regimes, are included in the mechanism but not optimized in this work.

The remaining reactions listed involve competing pathways for the carbon atoms without presence of oxygenated molecules as well as reactions causing $\mathrm{CH}_2\mathrm{O}$ production or destruction. We exclude the former from modification as we lack relevant species measurements to which to anchor; and we exclude the latter as these reactions are not specific to MMA kinetics and the rates are comparatively well-studied. Moreover, sensitivity analysis indicates that H-abstraction to the vinylic

pathway is much less significant than the allylic and alkylic pathways [23], and so we exclude (R5) from modification. To summarize, rate parameters for 4 reactions are optimized in this work, reflecting both initial decomposition (R1)–(R2) and H-abstraction reactions (R3)–(R4).

Fig. 9 shows the decomposition pathways including the targeted reactions and subsequent reactions leading to the targeted intermediate and product species. These pathways represent the most significant routes for CO, CO2, and CH2O production during MMA pyrolysis in the temperature ranges of interest in this chemical model. β -scission of the allylic and vinylic MMA radicals leads to CH₃OCO formation, from which both CO and CO2 are consequently produced, with CH2O an intermediate leading to CO. Alternately, H-abstraction of MMA to form the alkylic-position MMA radical has a distinct pathway leading via β scission to iC₃H₅CO and thereafter, CO. Thus, modifying the respective rates of the hydrogen abstraction reactions significantly impacts the resulting ratio of ${\rm CO}$ and ${\rm CO}_2$ produced. The Yang et al. detailed mechanism uses equal rates for the allylic and alkylic sites; the reduced Dakshnamurthy et al. mechanism differentiates the three H-abstraction reactions as the allylic radical is a relatively more stable molecule and the three abstraction sites have distinct related C-H bond dissociation energies (allylic < alkylic < vinylic) [23,58].

Though not explicitly detailed here, CH_3O becomes CH_2O via third-body collisions following its formation from CH_3OCO . After complete decomposition of CH_3OCO , reaction pathways to CO_2 are no longer available; however, CO continues to be produced by CH_2O following the typical route through the formyl radical, CO. This explains the fast plateau of CO_2 mole fraction seen at the higher temperatures (Figs. 5 and 6) while the mole fraction of CO continues to increase slightly at the expense of CH_2O .

4.2. Mechanism modification

As a next step beyond sensitivity analysis, an optimization procedure is employed to adjust the Arrhenius rate parameters for the

Table 1
Rate constants of the Dakshnamurthy et al. and the modified MMA pyrolysis models

	Reaction	Original parameters			Modified parameters		
		A	n	E	A	n	E
R1	MMA → iC ₃ H ₅ CO+CH ₃ O	9.55 ·10 ¹⁴	-0.39	369.0	4.36 ·10 ¹⁵	-0.49	350.1
R2	$MMA \rightarrow tC_3H_5+CH_3OCO$	$6.42 \cdot 10^{15}$	-0.35	350.6	$7.26 \cdot 10^{15}$	-0.37	305.2
R3	$MMA+H \rightarrow PJ+H_2$	1.86 ·10 ⁵	2.54	11.66	$2.06 \cdot 10^{6}$	2.69	5.84
R4	$MMA \! + \! H \rightarrow MJ \! + \! H_2$	$1.92 \cdot 10^{7}$	2.06	31.08	$1.55 \cdot 10^{8}$	2.21	35.86

A is in cm³ mol⁻¹ s⁻¹ or cm⁶ mol⁻² s⁻¹, E is in kJ mol⁻¹

target reactions. Often, shock tube pyrolysis studies aim to examine the decomposition rate of a molecular species at different temperatures, in order to determine elementary reaction rate constants based on pseudo-first-order kinetics [26]. This ideally involves direct timeresolved measurement of the decomposing species; however, with these measured product species time histories, we can compare the model predictions against experimental data and modify the Arrhenius rate parameters of the several targeted reactions to mitigate disagreement in the formation timescales and magnitudes observed. We focused here on selecting reactions from initial to early stages of decomposition and, in particular, reactions for which rate constants had relatively high levels of uncertainty in existing mechanisms. The rate parameters were optimized by employing a genetic algorithm-based method; the procedure followed is based on and detailed in the work of Sikalo et al. [29]. In each iteration - or generation - of the optimization, the sets of reaction rate parameters that minimize error between the measured and predicted species mole fraction (with equal weighting for CO and CO2) are selected. These best-performing solutions are then combined (some parameters from one solution set and merged with some from another set) and mutated (randomly selected parameter in a solution is varied) to be tested in the next iteration until a single solution is converged upon. Effectively, different permutations of the 12 Arrhenius rate parameters (for reactions (R1) through (R4)) are evaluated and improved upon until the experimental species timeevolutions can be reproduced by the kinetic model. The optimization was anchored to the first millisecond of test time of CO and CO2 speciation data. The CH2O data had higher uncertainty, and so was not weighted in the optimization; however, the improved agreement seen between the CH2O mole fraction measurements and the modified mechanism serves as a useful independent validation. The final modified rate parameters for the two unimolecular MMA decomposition reactions ((R1) and (R2)) and the key hydrogen abstraction reactions ((R3) and (R4)) are shown in Table 1. The resulting rates are shown as a function of temperature in Fig. 10.

The overall production of CO, CO2, and CH2O are all generally under-predicted by the Dakshnamurthy et al. mechanism compared to this speciation data; our mechanism optimization unsurprisingly resulted in rate increases for all targeted reactions. As the ratio of CO2 to CO produced and overall production are strongly affected by the rates of (R1) and (R2), these rates changed most significantly to better reflect the CO/CO2 observed in the shock tube experiments. For the abstraction reactions, the updated pre-exponential factors increased consistently by an order of magnitude for all of (R3) and (R4). The modified mechanism indicates that pre-exponential factors A for the targeted reactions should generally fall between those published in the Yang et al. and Dakshnamurthy et al. models. The optimization resulted in a near-negligible change to the temperature exponents n of the decomposition reaction ((R1) and moderate changes (<30%) for the other modified reactions ((R2), (R3), and (R4)). The activation energies E for the allylic site hydrogen abstraction reaction was decreased as were both of the decomposition reactions, falling between the values published in the Yang et al. and Dakshnamurthy et al. models for decomposition reactions ((R1) and (R2)) and lower than both existing models for the allylic H-abstraction (R3). Notably, the ordering of the activation energy and overall rate constant magnitudes remained

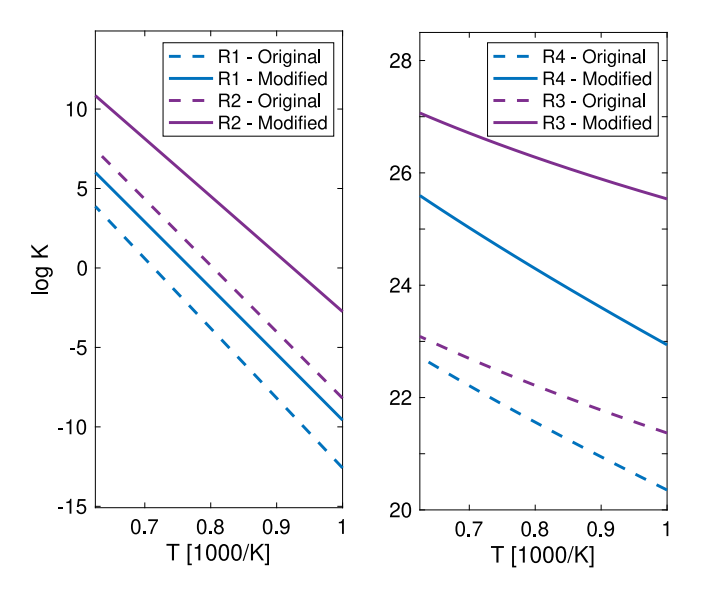


Fig. 10. Comparison of rates between the Dakshnamurthy mechanism and the modified mechanism for the unimolecular decomposition reactions of MMA (left) and hydrogen abstraction reactions (right).

unchanged for the abstraction reactions such as to follow the ordering of the relative C–H bond dissociation energies.

The predictions using the refined mechanism model are compared with the experimental species time-histories and existing mechanism in Figs. 5 and 6. The experimental and simulated mole fraction yields are shown in Fig. 7. As discussed in , the modified mechanism overall more closely predicts the experimental data of CO, CO2, and CH2O than either the unmodified version of the short MMA mechanism and the original detailed chemical model. However, the mole fraction magnitude agreement with the data worsens at the higher temperatures $(T_5 > 1500 \text{ K})$, particularly so for CO_2 and CH_2O . Both the detailed Yang et al. and the modified mechanisms predict the plateau level of the CO_2 mole fraction to be around X = 0.4% whereas we measure this to be around X = 0.6%. For CH_2O , we measure a more dramatic decline in mole fraction at $T_5 = \bar{1555}$ K than is captured by our modified model, though agreement is improved for the other four lower temperature tests for which CH2O was measured. Despite these magnitude discrepancies at select conditions, we observe good agreement in the time-evolution trends for all three measured species across the temperature range. Most notably, the modified mechanism shows significant improvement in capturing the initial highly temperaturedependent formation timescales of the decomposition products relative to both the Yang et al. and Dakshnamurthy et al. across all conditions. As a check on the impact of these changes regarding prior experimental works, flame speed predictions using the updated model were found to generally agree well with the flame speeds reported by Dakshnamurthy et al. with deviation ranging from 0.3%-8% over all conditions with an average disagreement of 4%. Comparisons of laminar flame speeds and species profiles can be found in the supplementary material. The modest differences observed between the models in laminar flame conditions highlights the enhanced sensitivity of the more targeted shock

tube pyrolysis studies performed in this work to the early decomposition reactions, which cannot be readily isolated in flame experiments. Overall, these kinetic rate adjustments represent a starting point in the refinement of a detailed mechanism for MMA oxidation. Future shock tube studies with oxidizing mixtures are expected to elucidate contributions of other reactions such as H-abstraction by O and OH.

5. Conclusion

In this work, the chemical kinetics of methyl methacrylate (MMA, C5H8O2) pyrolysis were examined in a shock tube reactor using infrared laser absorption spectroscopy. Experiments were conducted over a range of temperatures from 1200-1600 K and near atmospheric pressure. Quantitative interpretations of spectra obtained by laser absorption during the decomposition of MMA enabled species time-history measurements of carbon monoxide (CO), carbon dioxide (CO₂), and formaldehyde (CH₂O). The data were subsequently compared to existing models for MMA combustion, revealing significant disagreements. Guided by sensitivity analyses and genetic algorithm based optimization, we propose modified Arrhenius rate parameters for the two unimolecular decomposition reactions and key H abstractions that initiate MMA pyrolysis. Updating these rates within the short MMA mechanism of Dakshnamurthy et al. led to significantly improved agreement with speciation measurements. Some discrepant behavior still exists at higher temperatures that future experimental studies in different environments may reconcile. The data-driven insights and reaction mechanism improvements from this work are expected to help advance PMMA combustion models for hybrid rocket propulsion systems and fire science studies.

CRediT authorship contribution statement

Isabelle C. Sanders: Investigation, Methodology, Visualization, Validation, Formal analysis, Software, Writing – original draft, Writing – review & editing. Nicholas M. Kuenning: Investigation, Methodology, Software, Validation, Formal analysis. Nicolas Q. Minesi: Investigation, Methodology, Validation, Writing – review & editing. Daniel I. Pineda: Conceptualization, Methodology, Writing – original draft, Writing – review & editing. R. Mitchell Spearrin: Project administration, Conceptualization, Supervision, Funding acquisition, Writing – original draft, Writing – review & editing.

Declaration of competing interest

The authors declare that they have no known competing financial interests or personal relationships that could have appeared to influence the work reported in this paper.

Data availability

Data will be made available on request.

Acknowledgments

This work was supported by the U.S. National Science Foundation, CAREER Award No. 1752516 and by the Air Force Office of Scientific Research (AFOSR) Young Investigator Program (YIP) award no. FA9550-19-1-0062 with Dr. Chiping Li as Program Officer. ICS acknowledges support from the The Natural Sciences and Engineering Research Council of Canada. NQM acknowledges support from NASA's Space Technology Research Grants Program (award no. 80NSSC21K0066). The authors thank Denis Knyazkov for helpful discussion and sharing the short MMA mechanism files.

Appendix A. Supplementary data

Supplementary material related to this article can be found online at https://doi.org/10.1016/j.fuel.2022.126846. Supplementary document includes sample spectral data and further comparison of modified and exisiting MMA model performance.

References

- [1] Seshadri K, Williams FA. Structure and extinction of counterflow diffusion flames above condensed fuels: Comparison between poly(methyl methacrylate) and its liquid monomer, both burning in nitrogen-air mixtures. J Polym Sci Polym Chem Ed 1978;16(7):1755-78. http://dx.doi.org/10.1002/pol.1978.170160726, URL http://doi.wiley.com/10.1002/pol.1978.170160726.
- [2] Fernandez-Pello AC, Hirano T. Controlling mechanisms of flame spread. Combust Sci Technol 1983;32(1–4):1–31. http://dx.doi.org/10.1080/ 00102208308923650.
- [3] Zeng WR, Li SF, Chow WK. Review on chemical reactions of burning poly(methyl methacrylate) PMMA. J Fire Sci 2002;20(5):401–33. http://dx.doi.org/10.1177/0734904102020005482.
- [4] Kim S, Lee J, Moon H, Kim J, Sung H, Kwon OC. Regression characteristics of the cylindrical multiport grain in hybrid rockets. J Propuls Power 2013;29(3):573–81. http://dx.doi.org/10.2514/1.B34619.
- [5] Bhargava A, Van Hees P, Andersson B. Pyrolysis modeling of PVC and PMMA using a distributed reactivity model. Polym Degrad Stab 2016;129:199–211. http://dx.doi.org/10.1016/j.polymdegradstab.2016.04.016.
- [6] Fraters A, Cervone A. Experimental characterization of combustion instabilities in high-mass-flux hybrid rocket engines. J Propuls Power 2016;32(4):958–66. http://dx.doi.org/10.2514/1.B35485.
- [7] Mechentel FS, Hord BR, Cantwell BJ. Optically resolved fuel regression of a clear polymethylmethacrylate hybrid rocket motor. J Propuls Power 2020;1–10. http://dx.doi.org/10.2514/1.B37805.
- [8] Sanders IC, Bendana FA, Hagström CG, Spearrin RM. Injector effects on hybrid polymethylmethacrylate combustion assessed by thermochemical tomography. J Propuls Power 2021;37(6):928–43. http://dx.doi.org/10.2514/1.B38316, URL https://arc.aiaa.org/doi/10.2514/1.B38316.
- [9] Korting PA, Schöyer HF, Timnat YM. Advanced hybrid rocket motor experiments. Acta Astronaut 1987;15(2):97–104. http://dx.doi.org/10.1016/0094-5765(87) 00000-0
- [10] Thomsen M, Carmignani L, Rodriguez A, Scudiere C, Liveretou C, Fernandez-Pello C, et al. Downward flame spread rate over PMMA rods under external radiant heating. Fire Technol 2022;58(4):2229–50. http://dx.doi.org/10.1007/s10694-022-01245-y.
- [11] Xiong C, Fan H, Huang X, Fernandez-Pello C. Evaluation of burning rate in microgravity based on the fuel regression, flame area, and spread rate. Combust Flame 2022;237. http://dx.doi.org/10.1016/j.combustflame.2021.111846.
- [12] Rabinovitch J, Jens ET, Karp AC, Nakazono B, Conte A, Vaughan DA. Characterization of PolyMethylMethAcrylate as a fuel for hybrid rocket motors. In: 2018 joint propulsion conference. Reston, Virginia: American Institute of Aeronautics and Astronautics; 2018, p. 1–21. http://dx.doi.org/10.2514/6.2018-4530.
- [13] Ben-Yakar A, Natan B, Gany A. Investigation of a solid fuel scramjet combustor. J Propuls Power 1998;14(4):447–55. http://dx.doi.org/10.2514/2.5321, URL https://arc.aiaa.org/doi/10.2514/2.5321.
- [14] Westbrook CK, Pitz WJ, Curran HJ. Chemical kinetic modeling study of the effects of oxygenated hydrocarbons on soot emissions from diesel engines. J Phys Chem A 2006;110(21):6912–22. http://dx.doi.org/10.1021/jp056362g.
- [15] Yang B, Westbrook C, Cool T, Hansen N, Kohse-Höinghaus K. Photoionization mass spectrometry and modeling study of premixed flames of three unsaturated C5H8O2 esters. Proc Combust Inst 2013;34(1):443–51. http://dx.doi.org/ 10.1016/j.proci.2012.05.034, URL https://linkinghub.elsevier.com/retrieve/pii/ S1540748912000351.
- [16] Farooq A, Davidson D, Hanson R, Westbrook C. A comparative study of the chemical kinetics of methyl and ethyl propanoate. Fuel 2014;134:26–38. http: //dx.doi.org/10.1016/j.fuel.2014.05.035, URL https://linkinghub.elsevier.com/ retrieve/pii/S0016236114004888.
- [17] Wang H, Oehlschlaeger MA. Shock tube ignition delay time measurements for methyl propanoate and methyl acrylate: Influence of saturation on small methyl ester high-temperature reactivity. Int J Chem Kinet 2020;52(10):712– 22. http://dx.doi.org/10.1002/kin.21394, URL https://onlinelibrary.wiley.com/doi/full/10.1002/kin.21394, https://onlinelibrary.wiley.com/doi/abs/10.1002/kin.21394, https://onlinelibrary.wiley.com/doi/10.1002/kin.21394.
- [18] Westbrook CK, Pitz WJ, Westmoreland PR, Dryer FL, Chaos M, Osswald P, et al. A detailed chemical kinetic reaction mechanism for oxidation of four small alkyl esters in laminar premixed flames. Proc Combust Inst 2009;32 I(1):221–8. http://dx.doi.org/10.1016/j.proci.2008.06.106.
- [19] Ren W, Spearrin RM, Davidson DF, Hanson RK. Experimental and modeling study of the thermal decomposition of C3–C5 ethyl esters behind reflected shock waves. J Phys Chem A 2014;118(10):1785–98. http://dx.doi.org/10.1021/jp411766b.

- [20] Yang B, Westbrook CK, Cool TA, Hansen N, Kohse-Höinghaus K. Fuel-specific influences on the composition of reaction intermediates in premixed flames of three C5H10O2 ester isomers. Phys Chem Chem Phys 2011;13(15):6901–13. http://dx.doi.org/10.1039/c0cp02065f.
- [21] Wang T, Li S, Lin Z, Han D, Han X. Experimental study of laminar lean premixed methylmethacrylate/oxygen/argon flame at low pressure. J Phys Chem A 2008;112(6):1219–27. http://dx.doi.org/10.1021/jp709927j.
- [22] Lin Z, Wang T, Han D, Han X, Li S, Li Y, et al. Study of combustion intermediates in fuel-rich methyl methacrylate flame with tunable synchrotron vacuum ultraviolet photoionization mass spectrometry. Rapid Commun Mass Spectrom 2009;23(1):85–92. http://dx.doi.org/10.1002/rcm.3838, URL https:// onlinelibrary.wiley.com/doi/10.1002/rcm.3838.
- [23] Dakshnamurthy S, Knyazkov DA, Dmitriev AM, Korobeinichev OP, Nilsson EJ, Konnov AA, et al. Experimental study and a short kinetic model for high-temperature oxidation of methyl methacrylate. Combust Sci Technol 2019;191(10):1789–814. http://dx.doi.org/10.1080/00102202.2018.1535492.
- [24] Knyazkov DA, Bolshova TA, Shvartsberg VM, Chernov AA, Korobeinichev OP. Inhibition of premixed flames of methyl methacrylate by trimethylphosphate. Proc Combust Inst 2021;38(3):4625–33. http://dx.doi.org/10.1016/j.proci.2020. 06.048
- [25] Bolshova TA, Chernov AA, Shmakov AG. Reduced chemical kinetic mechanism for the oxidation of methyl methacrylate in flames at atmospheric pressure. Combust Explos Shock Waves 2021;57(2):159–70. http://dx.doi.org/10.1134/ S0010508221020040.
- [26] Law CK. Combustion physics. New York: Cambridge University Press; 2006.
- [27] Hanson R, Davidson D. Recent advances in laser absorption and shock tube methods for studies of combustion chemistry. Prog Energy Combust Sci 2014;44:103–14. http://dx.doi.org/10.1016/j.pecs.2014.05.001.
- [28] Bongartz D, Ghoniem AF. Chemical kinetics mechanism for oxy-fuel combustion of mixtures of hydrogen sulfide and methane. Combust Flame 2015;162(3):544–53. http://dx.doi.org/10.1016/j.combustflame.2014.08.019, URL https://linkinghub.elsevier.com/retrieve/pii/S0010218014002661.
- [29] Sikalo N, Hasemann O, Schulz C, Kempf A, Wlokas I. A genetic algorithm-based method for the automatic reduction of reaction mechanisms. Int J Chem Kinet 2014;46(1):41–59. http://dx.doi.org/10.1002/KIN.20826.
- [30] Niu B, Jia M, Xu G, Chang Y, Xie M. Efficient approach for the optimization of skeletal chemical mechanisms with multiobjective genetic algorithm. Energy Fuels 2018;32(6):7086–102. http://dx.doi.org/10.1021/acs.energyfuels.8b00356.
- [31] Won SH, Windom B, Jiang B, Ju Y. The role of low temperature fuel chemistry on turbulent flame propagation. Combust Flame 2014;161(2):475–83. http://dx. doi.org/10.1016/j.combustflame.2013.08.027.
- [32] Williams FA. A review of flame extinction. Fire Saf J 1981;3(3):163-75. http://dx.doi.org/10.1016/0379-7112(81)90041-2.
- [33] Bendana FA, Lee DD, Wei C, Pineda DI, Spearrin RM. Line mixing and broadening in the v(1→3) first overtone bandhead of carbon monoxide at high temperatures and high pressures. J Quant Spectrosc Radiat Transfer 2019;239:106636. http: //dx.doi.org/10.1016/j.jqsrt.2019.106636, URL https://linkinghub.elsevier.com/ retrieve/pii/S0022407319304042.
- [34] Pineda DI, Bendana FA, Schwarm KK, Spearrin RM. Multi-isotopologue laser absorption spectroscopy of carbon monoxide for high-temperature chemical kinetic studies of fuel mixtures. Combust Flame 2019;207:379–90. http://dx.doi. org/10.1016/j.combustflame.2019.05.030, URL https://linkinghub.elsevier.com/ retrieve/pii/S0010218019302433.
- [35] Campbell MF, Owen KG, Davidson DF, Hanson RK. Dependence of calculated postshock thermodynamic variables on vibrational equilibrium and input uncertainty. J Thermophys Heat Transfer 2017;31(3):586–608. http://dx.doi.org/10. 2514/174052
- [36] Gordon I, Rothman L, Hargreaves R, Hashemi R, Karlovets E, Skinner F, et al. The HITRAN2020 molecular spectroscopic database. J Quant Spectrosc Radiat Transfer 2022;277:107949. http://dx.doi.org/10.1016/j.jqsrt.2021.107949.
- [37] Rothman L, Gordon I, Barber R, Dothe H, Gamache R, Goldman A, et al. HITEMP, the high-temperature molecular spectroscopic database. J Quant Spectrosc Radiat Transfer 2010;111(15):2139–50. http://dx.doi.org/10.1016/j.jqsrt.2010.05.001.
- [38] Al-Derzi AR, Tennyson J, Yurchenko SN, Melosso M, Jiang N, Puzzarini C, et al. An improved rovibrational linelist of formaldehyde, H212C16O. J Quant Spectrosc Radiat Transfer 2021;266:107563. http://dx.doi.org/10.1016/j.jqsrt.2021. 107563. https://linkinghub.elsevier.com/retrieve/pii/S002240732100056X.

- [39] Kuenning NM, Sanders IC, Minesi NQ, Pineda DI, Spearrin RM. High-temperature absorption cross-sections of formaldehyde near 3.6 μm. J Spectrosc Radiat Transfer 2022 [in preparation].
- [40] Pine AS. Doppler-limited spectra of the CH stretching fundamentals of formalde-hyde. J Mol Spectrosc 1978;70(2):167–78. http://dx.doi.org/10.1016/0022-2852(78)90151-0.
- [41] McLean A, Mitchell C, Swanston D. Implementation of an efficient analytical approximation to the Voigt function for photoemission lineshape analysis. J Electron Spectrosc Relat Phenom 1994;69(2):125–32. http://dx.doi.org/10.1016/ 0368-2048(94)02189-7.
- [42] Fisher EM, Pitz WJ, Curran HJ, Westbrook CK. Detailed chemical kinetic mechanisms for combustion of oxygenated fuels. Proc Combust Inst 2000;28(2):1579–86. http://dx.doi.org/10.1016/S0082-0784(00)80555-X.
- [43] Akbar Ali M, Violi A. Reaction pathways for the thermal decomposition of methyl butanoate. J Organic Chem 2013;78(12):5898–908. http://dx.doi.org/10.1021/ icd00560d
- [44] Mendes J, Zhou CW, Curran HJ. Theoretical study of the rate constants for the hydrogen atom abstraction reactions of esters with oH radical. J Phys Chem A 2014;118(27):4889–99. http://dx.doi.org/10.1021/jp5029596.
- [45] Wang YL, Lee DJ, Westbrook CK, Egolfopoulos FN, Tsotsis TT. Oxidation of small alkyl esters in flames. Combust Flame 2014;161(3):810–7. http://dx.doi. org/10.1016/j.combustflame.2013.09.013, URL https://linkinghub.elsevier.com/ retrieve/pii/S0010218013003453.
- [46] Wang QD, Zhang W. Influence of the double bond on the hydrogen abstraction reactions of methyl esters with hydrogen radical: An ab initio and chemical kinetic study. RSC Adv 2015;5(84):68314–25. http://dx.doi.org/10.1039/ c5ra14880d.
- [47] Zhang L, Chen Q, Zhang P. A theoretical kinetics study of the reactions of methylbutanoate with hydrogen and hydroxyl radicals. Proc Combust Inst 2015;35(1):481–9. http://dx.doi.org/10.1016/j.proci.2014.05.117.
- [48] Huynh LK, Violi A. Thermal decomposition of methyl butanoate: Ab initio study of a biodiesel fuel surrogate. J Organic Chem 2008;73(1):94–101. http://dx.doi.org/10.1021/jo701824n.
- [49] Khaled F, Giri BR, Farooq A. A high-temperature shock tube kinetic study for the branching ratios of isobutene OH reaction. Proc Combust Inst 2017;36(1):265–72. http://dx.doi.org/10.1016/j.proci.2016.07.107.
- [50] Fenard Y, Dayma G, Halter F, Foucher F, Serinyel Z, Dagaut P. Experimental and modeling study of the oxidation of 1-butene and cis -2-butene in a jetstirred reactor and a combustion vessel. Energy Fuels 2015;29(2):1107–18. http: //dx.doi.org/10.1021/ef502732c.
- [51] Zhou CW, Li Y, O'Connor E, Somers KP, Thion S, Keesee C, et al. A comprehensive experimental and modeling study of isobutene oxidation. Combust Flame 2016;167:353–79. http://dx.doi.org/10.1016/j.combustflame.2016.01.021.
- [52] Gaïl S, Sarathy SM, Thomson MJ, Diévart P, Dagaut P. Experimental and chemical kinetic modeling study of small methyl esters oxidation: Methyl (E)-2-butenoate and methyl butanoate. Combust Flame 2008;155(4):635–50. http://dx.doi.org/10.1016/j.combustflame.2008.04.007.
- [53] Yasunaga K, Kuraguchi Y, Ikeuchi R, Masaoka H, Takahashi O, Koike T, et al. Shock tube and modeling study of isobutene pyrolysis and oxidation. Proc Combust Inst 2009;32 I(1):453–60. http://dx.doi.org/10.1016/j.proci.2008.06.
- [54] Es-Sebbar ET, Khaled F, Elwardany A, Farooq A. Rate coefficients of the reaction of OH with allene and propyne at high temperatures. J Phys Chem A 2016;120(41):7998–8005. http://dx.doi.org/10.1021/acs.jpca.6b04387.
- [55] Narayanaswamy K, Pitsch H, Pepiot P. A component library framework for deriving kinetic mechanisms for multi-component fuel surrogates: Application for jet fuel surrogates. Combust Flame 2016;165:288–309. http://dx.doi.org/10. 1016/j.combustflame.2015.12.013.
- [56] Goodwin DG, Moffat HK, Speth RL. Cantera: An object-oriented software toolkit for chemical kinetics, thermodynamics, and transport processes. 2018, http://dx.doi.org/10.5281/zenodo.170284.
- [57] Pineda DI, Bendana FA, Spearrin RM. Competitive oxidation of methane and C2 hydrocarbons discerned by isotopic labeling and laser absorption spectroscopy of CO isotopologues in shock-heated mixtures. Combust Flame 2021;224:54–65. http://dx.doi.org/10.1016/j.combustflame.2020.11.006, https://linkinghub.elsevier.com/retrieve/pii/S0010218020304971.
- [58] Blanksby SJ, Ellison GB. Bond dissociation energies of organic molecules. Acc Chem Res 2003;36(4):255–63. http://dx.doi.org/10.1021/ar020230d.